CONF-961005--23

GA–A22478

DIVERTOR PLASMA PHYSICS EXPERIMENTS ON THE DIII–D TOKAMAK

by
M.A. MAHDAVI, S.L. ALLEN, N.H. BROOKS, R. BASTASZ, L.R. BAYLOR, J.N. BROOKS, D. BUCHENAUER, J.W. CUTHBERTSON, T.E. EVANS, M.E. FENSTERMACHER, D.N. HILL, D.L. HILLIS, J. HOGAN, A.W. HYATT, R.C. ISLER, G.L. JACKSON, T. JERNIGAN, R. JONG, C.C. KLEPPER, R.J. LA HAYE, C.J. LASNIER, A.W. LEONARD, R. MAINGI, P.K. MIODUSZEWSKI, R.A. MOYER, M. MURAKAMI, L.W. OWEN, T.W. PETRIE, G.D. PORTER, M.E. RENSINK, T. ROGNLIEN, M.J. SCHAFFER, G.M. STAEBLER, R.D. STAMBAUGH, D.M. THOMAS, M.R. WADE, W.R. WAMPLER, J.G. WATKINS, W.P. WEST, D.G. WHYTE, C.P.C. WONG, R.D. WOOD, and The DIII–D PHYSICS and OPERATIONS TEAMS

RECEIVED
APR 03 1997
OSTI

MASTER

DISTRIBUTION OF THIS DOCUMENT IS UNLIMITED

OCTOBER 1996

GENERAL ATOMICS

DISCLAIMER

This report was prepared as an account of work sponsored by an agency of the United States Government. Neither the United States Government nor any agency thereof, nor any of their employees, makes any warranty, express or implied, or assumes any legal liability or responsibility for the accuracy, completeness, or usefulness of any information, apparatus, product, or process disclosed, or represents that its use would not infringe privately owned rights. Reference herein to any specific commercial product, process, or service by trade name, trademark, manufacturer, or otherwise, does not necessarily constitute or imply its endorsement, recommendation, or favoring by the United States Government or any agency thereof. The views and opinions of authors expressed herein do not necessarily state or reflect those of the United States Government or any agency thereof.

DISCLAIMER

Portions of this document may be illegible in electronic image products. Images are produced from the best available original document.

GA–A22478

DIVERTOR PLASMA PHYSICS EXPERIMENTS ON THE DIII–D TOKAMAK

by

M.A. MAHDAVI, S.L. ALLEN,* N.H. BROOKS, R. BASTASZ,† L.R. BAYLOR,‡ J.N. BROOKS,△ D. BUCHENAUER,† J.W. CUTHBERTSON,◊ T.E. EVANS, M.E. FENSTERMACHER,* D.N. HILL,* D.L. HILLIS,‡ J. HOGAN,‡ A.W. HYATT, R.C. ISLER,‡ G.L. JACKSON, T. JERNIGAN,‡ R. JONG,* C.C. KLEPPER,‡ R.J. LA HAYE, C.J. LASNIER,* A.W. LEONARD, R. MAINGI,¶ P.K. MIODUSZEWSKI,‡ R.A. MOYER,◊ M. MURAKAMI,‡ L.W. OWEN, T.W. PETRIE, G.D. PORTER,* M.E. RENSINK,* T. ROGNLIEN,* M.J. SCHAFFER, G.M. STAEBLER, R.D. STAMBAUGH, D.M. THOMAS, M.R. WADE,‡ W.R. WAMPLER,† J.G. WATKINS,† W.P. WEST, D.G. WHYTE,§ C.P.C. WONG, R.D. WOOD,* and The DIII–D PHYSICS and OPERATIONS TEAMS

This is a preprint of a paper to be presented at the Sixteenth IAEA International Conference on Plasma Physics and Controlled Nuclear Research, October 7–11, 1996, Montreal, Canada, and to be published in *The Proceedings.*

*Lawrence Livermore National Laboratory, Livermore, California.
†Sandia National Laboratories, Livermore, California.
‡Oak Ridge National Laboratory, Oak Ridge, Tennessee.
△Argonne National Laboratory, Argonne, Illinois.
◊University of California, San Diego, California.
¶Oak Ridge Associated Universities, Oak Ridge, Tennessee.
§INRS — Energie et Materiaux, Varennes, Quebec, Canada.

Work supported by
the U.S. Department of Energy under Contract Nos.
DE-AC03-89ER51114, DE-AC05-96OR22464, W-7405-ENG-48,
W-31-109-ENG-38, DE-AC04-94AL85000, and Grant No. DE-FG03-95ER54294

GA PROJECT 3466
OCTOBER 1996

GENERAL ATOMICS

F1-CN-64/A4–3

ABSTRACT

DIVERTOR PLASMA PHYSICS EXPERIMENTS ON THE DIII–D TOKAMAK.

In this paper we present an overview of the results and conclusions of our most recent divertor physics and development work. Using an array of new divertor diagnostics we have measured the plasma parameters over the entire divertor volume and gained new insights into several divertor physics issues. We present direct experimental evidence for momentum loss along the field lines, large heat convection, and copious volume recombination during detachment. These observations are supported by improved UEDGE modeling incorporating impurity radiation. We have demonstrated divertor exhaust enrichment of neon and argon by action of a forced scrape off layer (SOL) flow and demonstrated divertor pumping as a substitute for conventional wall conditioning. We have observed a divertor radiation zone with a parallel extent that is an order of magnitude larger than that estimated from a 1-D conduction limited model of plasma at coronal equilibrium. Using density profile control by divertor pumping and pellet injection we have attained H–mode confinement at densities above the Greenwald limit. Erosion rates of several candidate ITER plasma facing materials are measured and compared with predictions of a numerical model.

1. INTRODUCTION

Until recently, The DIII–D divertor data base was limited to upstream SOL parameters and plasma parameters at the target plate. Using the new and existing diagnostic systems of the DIII–D, in a recent experimental campaign we have extended the divertor data base to the bulk of the divertor plasma. We have made 2-D maps of the parameters of the divertor plasma from the inner strike point to the outer strike point and from the target plates to above the X–point [1–5]. The new dedicated divertor diagnostic systems [6–12] include: a divertor Thomson scattering system (TS), a fast scanning Langmuir probe (FSLP), and EUV and visible spectrometers, and a Penning gauge (Fig. 1). For the first time we have the capability for local transport studies in the divertor plasmas and can readily obtain a measure of the local values of parallel conducted heat flux $q_{||} = \kappa_{||} T^{5/2} \partial T / \partial x_{||}$. A radially averaged measure of the local radiated power density is obtained from inversion of a 48 channel bolometer array data which combined with spectroscopic results has identified the dominant radiative impurities and additional channels of heat transport. The data from these diagnostics can severely test the validity of divertor plasma models.

The Thomson scattering and the scanning Langmuir probe systems measure T_e and n_e along a vertical path at the major radius of 1.48 m above the vessel floor. Time resolution of the measurements are 2 and 0.5 ms respectively By sweeping the divertor plasma across the measurement location of these two diagnostics two dimensional distributions of the plasma parameters have been obtained.

Broad spectral coverage of the DIII–D divertor is provided by an XUV SPRED and a visible survey spectrometer. In addition, two multichordal visible spectrometers with high spectral resolution give information on the radial distribution and the Doppler broadening of impurity ions.

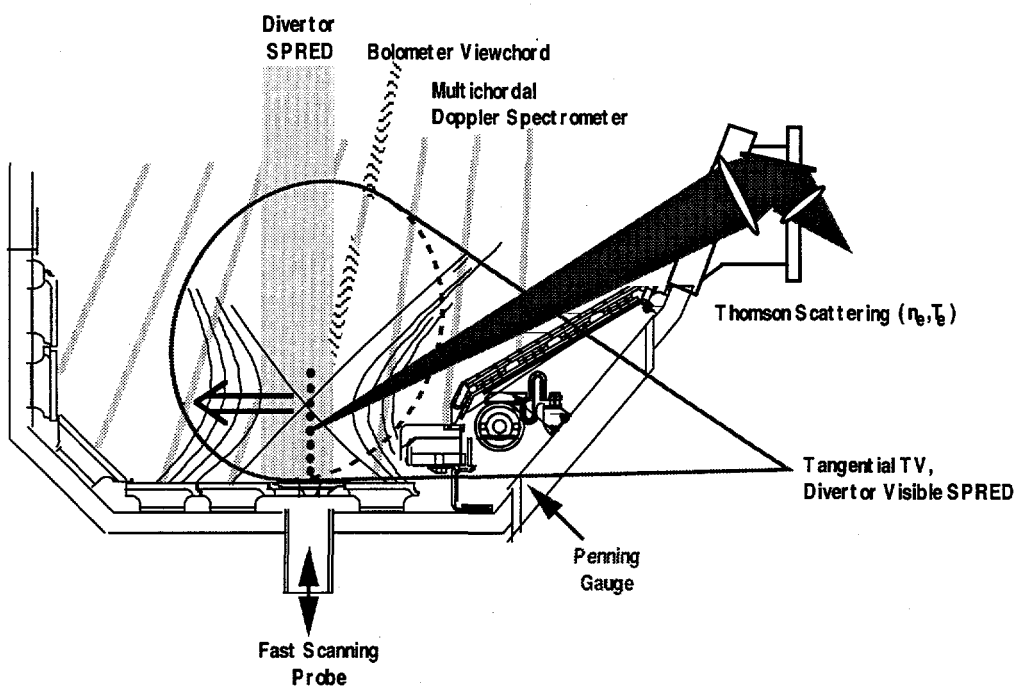

Fig. 1. A Cross section view of the lower section of the DIII–D vessel showing the views of new divertor diagnostics. The plasma is swept radially to obtain a two dimensional map of the divertor plasma parameters.

These diagnostics are complemented with the existing DIII–D diagnostics. These systems provide: n_e and T_e in the SOL from the outer channels of the core Thomson system, and from target plate Langmuir probes; SOL T_i from Charge Exchange Recombination spectroscopy, radiated power from a 48 channel bolometer array, target plate heat and particle flux from an infrared TV, spectrally filtered 2-D images of the divertor plasma from tangentially and vertically viewing visible cameras, D_α light from arrays of fast photo diodes, and neutral pressure measured by ASDEX gauges.

Intermediate to high recycling radiative divertor conditions were measured in Ohmic, L–, and ELMing H–mode plasmas. The radiative modes studied are partially detached divertor, induced by D_2 puffing, and enhanced radiation with impurities, induced by neon or nitrogen injection. This data provides direct evidence for electron pressure drop along the field lines and evidence of copious volume recombination in detached plasmas (Section 3).

The UEDGE [13] code contains a 2-fluid model of the plasma with multi-species ions, classical parallel heat flux, anomalous perpendicular transport, and a Navier-Stokes fluid model of neutrals which permits momentum loss by charge exchange. The extensive data obtained recently is being used to examine the validity of physics models in UEDGE[14,15], and a Monte Carlo impurity (MCI) code [16]. In Section 3 we compare results of a UEDGE code simulation and experimental data from a detached plasma.

A powerful tool for enhanced divertor performance in ITER and other next generation devices is divertor pumping. We have used divertor pumping for divertor impurity enrichment, developing an extended divertor radiative zone, as a wall condi-

tioning substitute for the conventional helium glow discharge cleaning, and to access densities above the Greenwald limit in H–mode (Section 4).

Performance of a radiative divertor might be enhanced by divertor impurity enrichment. In a series of experiments simultaneous SOL gas puffing and divertor pumping were used to establish a SOL flow in order to preferentially concentrate the radiating impurities in the divertor plasma. In Section 4 we present the results of the so called "puff and pump" experiments where we have obtained direct evidence of plenum impurity enrichment.

Helium glow discharge cleaning (HeGDC) is one of the most effective wall conditioning tools in present day short pulse tokamaks. However, this technique is not applicable to long pulse devices. We have demonstrated that divertor pumping, which is applicable to long pulse operation, is an effective substitute for HeGDC (Section 4).

An overwhelming body of tokamak data that roughly agrees with the so called empirical Greenwald density limit scaling: $n_e < 10^{14} \times I_p / \pi a^2$ m^{-3}. In ITER, both to achieve a radiative divertor and ignition require operating at a line average density of ~1.5 times the Greenwald limit. We have shown that density profile control is a key to achieving high confinement at high densities. Using a combination of divertor pumping and pellet injection, we have obtained H–mode plasmas with a confinement of 1.8×ITER–89P at a regulated density of 1.5× Greenwald limit (Section 4).

A steady state model of the divertor plasmas might not be adequate for describing the divertor plasma behavior for calculating the life time of the divertor target materials. The divertor plasma properties can be inherently time dependent, as was seen in high density DIII plasmas [17], or be modulated by transient heat or particle pulses of ELMs and other events originating in the core plasma. In order to estimate divertor heat and particle fluxes due to ELMs in ITER we have measured ELM energy losses in the main plasma and the resulting heat and particle flux in the divertor (Section 5).

In a long pulse tokamak the life time of the divertor plate might be determined by the net erosion rate of the divertor material. We have measured erosion rates of several candidate divertor materials for ITER using the Divertor Material Evaluations Studies system (DiMES).

2. CHARACTERISTICS OF ATTACHED AND DETACHED PLASMAS

Here we will discuss the results and conclusions from a subset of the recent data containing moderate recycling and highly radiative detached plasmas induced by gas puffing [1–5,18]. Discharge parameters were in the following ranges: I_p = 0.9 to 1.5 MA, B_T = 2.1 T, P_{inj} = 1 to 10 MW, q_{95} = 3.7 to 6.6, and the $\nabla \mathbf{B}$ drift toward the divertor. Radial sweeps of the divertor plasma were used to allow diagnostics with vertical views to sample the entire divertor plasma. For this work it is assumed that conditions in the divertor remain nearly constant as the plasma is moved since the configuration is essentially an open divertor on horizontal targets without pumping throughout the sweep.

The divertor plasma parameters in the outer leg of moderate recycling ELMing H–mode plasmas display the classical characteristics of conduction limited heat flow in the SOL. The regions of significant radiated power are in the inner divertor leg and SOL. The radial profile and magnitude of the electron pressure remain roughly constant throughout the SOL while electron temperature decreases monotonically towards the plate. The radial profile and absolute values of n_e and T_e in the vicinity of the X–point are nearly the same as the corresponding midplane values. At the outer strike point, the density is ~3 times the X–point value, while T_e is reduced from the X–point value by the same factor. The transverse profiles of the electron density and

temperature remain roughly invariant throughout the SOL. The parallel heat flux obtained from the gradient of the electron temperature along a flux surface corresponding to peak heat flux at the target plate is roughly constant along the field lines, which is consistent with low radiation in this region. At the separatrix however the conduction heat flux decreases by a factor of 2 from the X–point to the vicinity of the target plate, which is indicative of radial transport at the sharp boundary between the SOL and the private flux region.

The behavior of high recycling partially detached plasmas is qualitatively different from the previous case. The regions of significant radiated power shift to the vicinity of the X–point and outer leg, and the peak heat flux at the divertor target drops a factor of 3–5. Typical reconstructions of total radiated power from the bolometer arrays and IR measurement of divertor heat flux are shown in Fig. 2 at times before and during the partial detachment. In heavy puffing discharges the carbon emission coalesces outside the separatrix near the X–point although the core energy confinement is not affected. For very heavy puffing the peak in the visible carbon radiation appears inside the last closed flux surface above the X–point and the energy confinement of the core plasma is reduced.

In detached plasmas [18–32] the electron pressure is not constant along the field lines and parallel heat conduction does not always dominate heat transport down stream. Near the separatrix the pressure decreases by an order of magnitude from the midplane to the vicinity of the target plate; whereas, farther out radially pressure remains constant or increases towards the plate. Most of the pressure variation occurs below the X–point. The pressure profile at the target plate peaks outboard of the separatrix where it is a factor of 3–5 greater than the separatrix value. In the vicinity of the separatrix, electron density increases at the X–point elevation to 10 times its midplane value , but then decreases towards the plate where it becomes comparable to the midplane value. Farther out in the SOL, electron density increases monotonically to $\sim 5 \times 10^{20}$ m^{-3} near target, 10 times the corresponding midplane value. In the vicinity of the separatrix, the electron temperature drops by more than an order of magnitude to 1–2 eV at the target plate. Most of the temperature drop occurs above the X–point. In the region below the X–point, parallel heat flux, estimated from the average gradient of the electron temperature is negligible compared to the moderate recycling case, discussed above. The same qualitative behavior is seen in lower power detached L–mode plasmas; except for lower densities in the cold areas. Profiles of electron density and temperature in a detached L–mode shot are shown in Fig. 3. There is an apparent discrepancy between this observation and observation of significant radiated power downstream. The resolution of this discrepancy is addressed in a later paragraph.

Spectroscopy data show that carbon and deuterium are the sources of almost all the divertor radiation[10,33,34]. Near the target plate carbon and deuterium radiation are roughly equal. However, total carbon radiation is three times greater than that of deuterium. The total power radiated per cm^2 deduced from spectroscopy agrees well with that detected from a bolometer with a slightly different field of view.

As an independent check on the effective electron temperatures derived from the ratios of XUV lines we have measured ion temperatures for C II and C III from Doppler broadening of visible lines taking into account the exact magnetic sub-level splitting caused by the Zeeman/Paschen-Bach effect. For C II, effective electron temperatures in the range 2–4 eV have been observed, with ion temperatures typically 1–2 eV lower. For C III, where the characteristic thermalization time can be much smaller than the ionization time, electron and ion temperatures are generally in good agreement, ranging from 6 to 15 eV depending on plasma conditions.

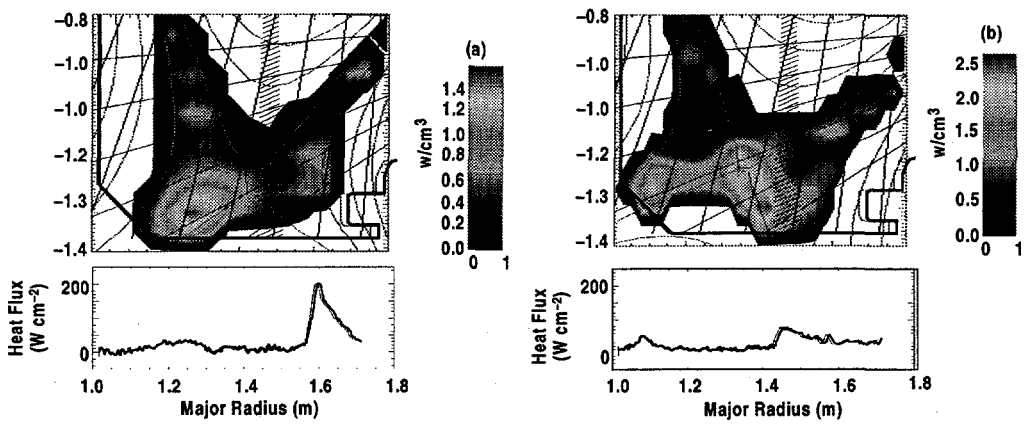

Fig. 2. Gray scale images of the plasma emissivity, before (a) and after detachment (b), reconstructed from the data from a 48 channel bolometer array. The figure also shows the corresponding profiles of heat flux to the divertor plate. After gas puffing the region of significant radiated power shifts from the inner divertor leg to the outer leg while the peak heat flux at the outer leg drops by a factor of 3.

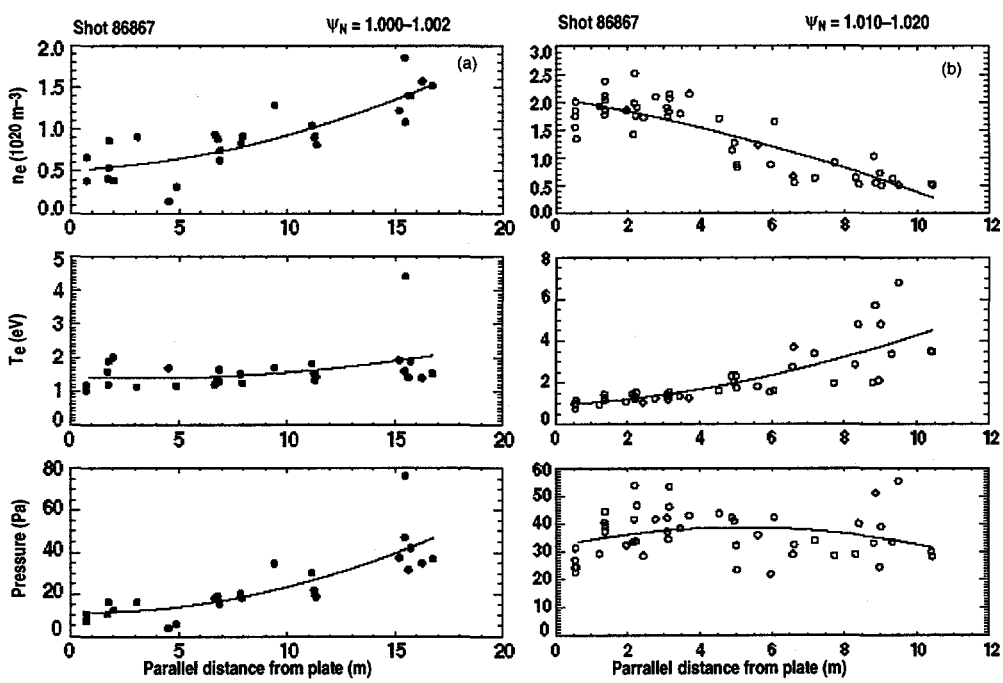

Fig. 3. Profiles of the electron temperature, density, and pressure, along the field lines in a region between the X-point and the target plate, measured by the divertor Thomson scattering system during a detached L-mode shot. The solid circles represent data from vicinity of the separatrix (y = 1.001-1.003) and the open circles represent data from a flux surface within the SOL (y = 1.010–1.020). Near the Separatrix the electron pressure drops by a factor of 5 from X-point to the plate, whereas the pressure is roughly constant farther out in the SOL.

3. DISCUSSION AND MODELING

In general, the UEDGE code produces all experimentally observed divertor states [14,15] : fully attached, detached at the inner strike point, detached at both strike points, and ultimately a core MARFE. Detached states are produced at low power pure deuterium plasmas or at high power plasmas with impurity radiation. The code accurately simulates attached plasmas, with a good match of the SOL profiles at the midplane, near the X–point and in the divertor. In the following we will discuss in more detail a comparison of code results with the experimental data from a detached plasma. Although quantitative agreement between the simulation and experiment is not as good as for attached plasmas, the code solution identifies the physical processes which dominate the behavior of detached divertor plasmas.

The simulation which uses a fixed fraction impurity model and the measured core plasma parameters and input power, matches the midplane temperature profile well. The simulated SOL density profile is slightly broader than the experiment. These simulations show a target plate temperature of 1 eV, in agreement with the Thomson measurement. In the simulation, the 5 eV temperature contour (ionization front) is clearly upstream from the divertor plates by ~6 cm in the outer leg [Fig. 4(a)] and 14 cm in the inner leg; however, divertor Thomson scattering data for the outer leg shows this front to be 10 cm away from the plate on the outer leg. The UEDGE simulation produces more hydrogenic radiation than carbon radiation, whereas spectroscopy suggests that carbon radiation is twice the deuterium line emission.

In the simulation, plasma momentum loss occurs in two steps. First, in the region of 5–15 cm above the plate a large local particle source converts roughly one half of the upstream plasma pressure into parallel flow momentum [23] with the Mach number approaching unity [Fig. 4(b)]. Since most of the heat dissipation takes place at or above the X–point whereas most of the pressure drop occurs below the X–point, it seems that the mechanisms for the pressure drop and heat dissipation are not directly coupled, although a low temperature caused by radiation is a likely prerequisite for the momentum loss process. In the second step, ion neutral interactions transfer most of the directed flow momentum to the vessel walls. Volume recombination in this simulation is as high as 1.5×10^{25} m^{-3}/s near the plate with a volume integral which is 3 times the total plate ion current.

Hydrogenic radiation from this recombination offers a qualitative explanation for the apparent discrepancy between the observation of a region of high emissivity below the 5 eV ionization front and very low conduction heat flux based on the low electron temperatures (1–3 eV) and temperature gradient ($\lesssim 1$ eV m^{-1}), measured by Thomson scattering. The near sonic flow towards the plate convects a substantial amount of thermal energy and a comparable or greater amount of ionization potential energy. In the regions where $T_e \sim 1$ eV and $n_e \sim 5\times10^{20}$ m^{-3}, the plasma recombines through three body recombination, since the three body recombination rate is an order of magnitude greater than the ionization and radiative recombination rates. Since the recombination is mainly into high n levels which subsequently decay to the ground state by line emission, most of the ionization potential is converted into hydrogenic line emission. This interpretation is consistent with the experimental observation that deuterium is the dominant radiating species near the plate.

Another possible explanation for the observed radiation in the cold plasma region is a burst of heat during ELMs. Since, presently, the Thomson data is taken between ELMs, the conduction heat flux during ELMs is not resolved. However, normally bolometric data is averaged over several ELMs.

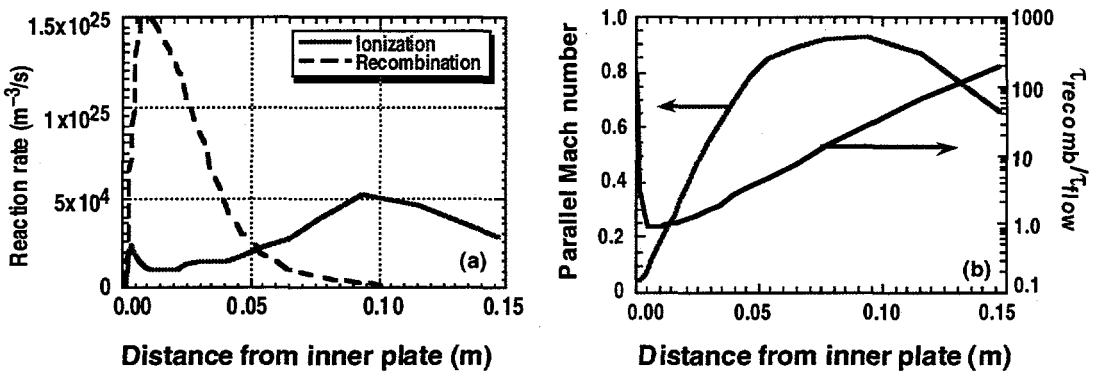

Fig. 4. UEDGE simulation results for a detached plasma using a fixed fraction impurity model. The code results show that the ionization is approximately 10 cm centimeters away from the plate and that a region of strong volume recombination has developed near the target plate(upper box). The upstream ionization causes a flow towards the plate that reduces the plasma pressure and convects heat(lower box).

4. DIVERTOR PERFORMANCE ENHANCEMENT

Feasibility of a radiative divertor depends critically on the achievable ratio of impurity concentration in the divertor relative to the core plasma and on the emissivity of the radiating impurity in the divertor plasma environment. SOL flows play a key role both in the process of divertor impurity enrichment and in the process of increasing impurity emissivities above the coronal equilibrium. In this section we present results of experiments on both impurity enrichment and spatial extension of the divertor radiative.

4.1. Divertor Impurity Enrichment by a Forced SOL Flow

A plasma flow in the direction of the target plate tends to drag impurities down stream, opposing the temperature gradient force [35,36] which tend to drives impurities upstream towards the core plasma. A sufficiently strong forced flow, established by simultaneous gas puffing in the SOL and divertor pumping, can thus increase the impurity concentration in the divertor plasma relative to the core. In the high recycling regime, a large plasma flow occurs naturally within an ionization mean free path of the recycling neutrals. The effect of this flow on impurity exhaust was demonstrated in the DIII device and ASDEX-U [35,37,38]. However, the range of recycling flows is normally limited to the vicinity of the divertor target, whereas it is desirable to have a significant flow throughout the radiating volume of the divertor plasma to oppose the forces which drive impurities upstream. A forced SOL flow, albeit smaller than the recycling flows, can be more effective upstream where recycling flux is low. Earlier DIII–D experiments [39] demonstrated that a forced SOL flow is compatible with a steady state constant density core plasma. The same experiments also showed that this 'puff and pump' approach was effective in reducing the argon content in the core plasma, but the results were somewhat inconclusive because the analysis was based on indirect measurements of the core argon content and there were no divertor argon measurements.

The experiments presented here [40] featured direct measurements of core plasma and exhaust gas impurity densities. Neon and argon concentrations in the core plasma

are obtained from measurements of the charge-exchange excited transitions. A modified Penning gauge provides simultaneous measurements of deuterium, helium, neon, and argon partial pressures in the divertor pumping plenum [41,42]. Divertor impurities are monitored by the divertor SPRED instrument that views through the main plasma and the lower divertor along a vertical chord. Trace impurity contents in the various reservoirs of two nearly identical discharges, one of which has D_2 injected from a single gas valve at the top of the machine and one with the same amount of D_2 injected into the divertor private flux region, are compared. The core and divertor plasma density are maintained the same in the two cases by controlled divertor pumping, so that the effect of other forces responsible for impurity transport in the SOL and divertor (e.g., divertor recycling, parallel temperature gradients. etc.) are maintained constant. This particular comparison allows one to distinguish the effect of SOL flow, since the top fueling case will have SOL flow and divertor recycling, whereas the divertor fueling case will mainly have divertor recycling. In all cases the impurity injected into the divertor private flux region. The results of such experiments are summarized in Table I. Two different deuterium flow levels, 80 and 150 torr-ℓ/s, were used for each of the impurities. For both impurities, the top fueling case consistently yields higher exhaust impurity enrichment than divertor fueling, showing that SOL flow indeed has an impact on divertor retention of impurities. The effect is particularly strong with argon where a relative enrichment of 7 is obtained. With argon, one also observes a factor of two relative enrichment with the increased level of D_2 injection even with divertor fueling.

Table I. Summary of Experiments on Impurity Enrichment By a Forced Flow

D_2 Flow Location	Top	Divertor	Top	Divertor
Flow (Torr-l/s)	150	150	80	80
Line-Averaged Density	6.2×10^{19}	6.1×10^{19}	6.0×10^{19}	6.1×10^{19}
Plenum Pressure (mTorr)	4.0	3.5	1.6	1.5
ELM Frequency (Hz)	60	55	60	55
Neon Enrichment	1.4	1.0	1.2	1.0
Argon Enrichment (Relative)*	6.9	2.2	1.7	1.0

*Normalized to enrichment in 80 Torr-l/s divertor fueling.

4.2. Extension of Divertor Radiating Zone

Deviations from coronal equilibrium can increase impurity emission relative to coronal equilibrium several orders of magnitude [43]. Several authors [44,45] have suggested that it may be feasible to take advantage of such emissivity enhancements in a radiative divertor. Two processes contributing to radiation enhancement are charge exchange reactions with neutrals or rapid recycling of the impurities. The emissivity enhancement occurs mainly at temperatures above the first burnout temperature of the impurity. In a divertor plasma, enhanced non coronal radiation in essence would extend the high radiation zone upstream to areas of higher temperature where the radiative impurity is normally burned out. Both effects that lead to enhanced emissivity necessitate a large SOL flow. Furthermore, the convected heat flux due to this flow can limit the achievable heat flux reduction be non-coronal radiation [46]. However,

heat convection can have a beneficial effect. Convection enhances heat transport along the field lines, thus would allow low temperature impurities to radiate from a larger volume than with pure conduction. A modest divertor heat flux reduction gained from these two effects combined might be sufficient for the success of a radiative divertor in ITER [45].

In a recent experiment [47] we have observed a radiative zone with a poloidal extent which is an order of magnitude greater than that expected from coronal radiation and conduction limited heat flow along the field lines. The experiment was performed in a configuration with a poloidal X–point-to-target plate distance of ~50 cm, which was six times the spatial resolution of the bolometer array diagnostic. The configuration has the additional advantage of providing a wide channel outside of the divertor plasma for the recycling particles to reach deep into the divertor volume. Deuterium gas was injected into the divertor of an ELMing H–mode plasma at a rate of 190 torr-ℓ/s to increase radiative losses and thereby decrease the divertor target heat flux. The radiative losses increased to 65% of the 10 MW of the input power. The 2D distribution of radiative losses is deduced from the bolometer array data. Over the entire outboard leg of the divertor, variation of the radiated power along the divertor channel is less than a factor of 2.

Assuming a one dimensional geometry and no convection, we have obtained the distribution of the parallel heat flux by integrating the radiated power density from the divertor plate to the X–point. Our results show that the parallel heat flux in the outboard divertor leg drops from an initial value of 100 MW/m^2 at the X–point to 45 MW/m^2 at the target plate, over a distance of 10 m. Furthermore, by substituting the heat flux into the heat conduction equation and integrating along the field lines, we have obtained an upstream electron temperature of 50 eV. Spectroscopic results show that carbon is the dominant radiative impurity in these plasmas. However, under these conditions, carbon radiation in coronal equilibrium would produce a radiation zone 10 times shallower than observed. This conflict could be resolved by allowing non-coronal radiation. A second possibility is that in a large segment of the SOL convection transports energy downstream faster than conduction, allowing a more extended radiating zone.

4.3. Wall Conditioning by Divertor Pumping

Divertor and vessel wall materials can absorb or release large quantities of particles, far greater than the plasma particle inventory [48]. In present day pulsed plasmas Helium Glow Discharge cleaning (HeGDC) is commonly used to minimize the wall particle inventory and thereby uncontrolled plasma fueling by wall released particles. An experiment was conducted to evaluate the feasibility of continuous divertor pumping as a substitute for the transient HeGDC between plasma discharges to maintain a low recycling wall in steady state plasmas [49,50]. After obtaining reference discharges with HeGDC, a sequence of 12 discharges was conducted without HeGDC and with the divertor cryopump "off". Particle balance analysis shows that the net wall inventory was increased by 1250 torr-ℓ (9×10^{22} atoms) during this phase. Assuming uniform deposition of the particles over the 60 m^2 of (type?) graphite in the DIII–D, this quantity corresponds to an average of 60 monolayers or alternatively to a saturated layer (i.e. 0.4 deuterons per carbon atom) of 150 Å depth. The divertor cryopump was then activated for the next 10 discharges. Two separate estimates of the cryopump exhaust rate were made, based on pump plenum measurements from a fast time-response ionization gauge and a slower time response capacitance manometer indicated that the wall inventory was reduced near to or below the reference level at the

end of the of the first discharge sequence. Plasma stored energy measured during the steady ELMy phase of each discharge was reduced by 15% on the first discharge without HeGDC and was restored to the reference level on the first discharge with active pumping. Thus, continuous particle exhaust by the divertor cryopump is shown to maintain low recycling, good performance conditions in the absence of HeGDC.

4.4. Access to High Densities

We have embarked upon a series of experiments to understand the physics of density limit in tokamak plasmas and to devise a path for ITER to reach densities 50% above the Greenwald limit [51–54] ($n_{\mathbf{max}}^{\mathbf{GW}} \sim I_p / \pi a^2$) required for ignition and safe divertor operation. This density must be achieved in moderately high performance ITER plasmas [55] with H=2,q_{95} =3 , and β_N=2. The essential tools to accomplish this effort are a pellet injector, the Advanced Divertor cryopump, and arrays of high resolution diagnostics that measure profiles of electron density and temperature, ion temperature, impurity concentration and current profile. Up to this point in time, our highest quasi-steady (≥0.4 s) line-average density has been 50% above $n_{\mathrm{max}}^{\mathrm{GW}}$, with global energy confinement times of 1.8, normalized to the ITER89P scaling. The highest transient density obtained in L–mode discharges was $3 \times n_{\mathrm{max}}^{\mathrm{GW}}$. Analysis of the data shows that there is no fundamental obstacle to achieving line average densities above the Greenwald limit. However, there are numerous resolvable ones that make the path to high densities very difficult. In absence of divertor pumping, divertor density increases non linearly with line average density and ultimately results in the collapse of the divertor plasma. This obstacle was readily removed by divertor pumping to control the divertor plasma density. In contrast to ref.[51], it is found that the density relaxation time after pellets is largely independent of the density relative to the Greenwald limit; although, pellets generally trigger ELMs and in some regimes cause H– to L–mode transitions which eject most of the pellet particles.

Radiation driven instabilities, such as MARFE [56], within the core plasma can in principal prevent access to the desired densities. We have demonstrated that densities well above Greenwald can be reached with a modest heating power at q~3 without MARFE instability. Conversely, MARFEs were produced below the Greenwald limit at high q operation. Core radiation limits have been encountered at low auxiliary heating power and densities $1.5–3 \times n_{max}^{\mathrm{GW}}$. In all such cases off axis absorption of the neutral beam power due to high density was the main factor leading to radiative collapse of the core plasma.

Large amplitude MHD modes frequently prevent access to desired densities. Analysis of Mirnov oscillations show growth of rotating tearing-type modes (m/n=2/1) when the injected pellets cause a large density perturbations. These modes often reduce energy and particle confinement back to L–mode levels and occasionally lock and cause a disruption. These modes are normally observed at moderate to high densities. However, at times they are stabilized with further density increase.

5. ELMs

The difficult engineering of the plasma facing components of future high powered long pulse devices is further aggravated by the transient high heat and particle fluxes during ELMs [57-61]. In order to estimate divertor heat and particle fluxes due to ELMs in ITER we have measured ELM energy losses in the main plasma and the resulting heat and particle flux in the divertor [57]. These ELM measurements were made in single null plasmas during the quasi steady state phase of ELMing H–mode.

The auxiliary heating power was varied from 2.5 MW to 12.0 MW at plasma currents of 1.0 to 1.8 MA. At a toroidal field of 2.1 T, the current scan yielded a q_{95} range of 3.6 to 6.4.

Loss of energy per ELM was determined from diamagnetic measurements. Over the entire parameter regime the average energy loss per ELM varies from about 20 kJ to 70 kJ with an ELM frequency varying proportional to the injected power at 10 to 100 Hz . Roughly, the energy loss per ELM is constant with injected power and increases with plasma current. The fractional ELM energy loss, the ELM energy divided by the main plasma stored energy, is found to scale inversely with the injected power normalized by a parameter related to the H–mode power threshold, the product of the toroidal field and the plasma surface area. For a given set of parameters individual ELM energy loss may vary by more than a factor of two. The standard density dependence to the H–mode power threshold scaling has been removed because it relates to the density before the H–mode transition, not the density the H–mode eventually achieves. An ELM energy scaling, derived from a combination of DIII–D and ASDEX-Upgrade data, predicts a 3% energy loss for ITER, or 35 MJ.

Divertor heat flux is measured by IR cameras at two toroidal positions. The ELM heat deposition profiles at the target plate are flatter and less peaked than the quiescent profiles, but remain localized to the same region of the divertor. The inboard divertor ELM energy deposition accounts for ~11% of the injected power and the outboard ~10%. One half to all of the main plasma energy loss measured by diamagnetism is deposited on the divertor plates as heat flux. Bolometric measurements indicate that ≤15% of the ELM energy is radiated away, mostly in the divertor. The scatter in energy accountability, 50%–100%, is in large part due to measurement limitations. A comparison of the data from the two IR cameras indicates that the toroidal peaking factor is usually less than 1.5 when integrated over the entire ELM heat flux. Previous measurements of divertor tile currents on DIII–D [62] have shown greater toroidal asymmetry than this, but on a faster timescale.

Divertor particle fluxes are deduced from the saturation current of an array of divertor floor Langmuir probes. The particle flux profile during the quiescent period between ELMs is seen to peak near the separatrix with a spatial width similar to the quiescent heat flux. During an ELM the instantaneous particle flux can increase a factor of 10–50. However, because of the short ELM duration the increase in time-averaged particle flux due to ELMs is of the same order as that of the background during the quiescent periods. The ELM particle flux spatial distribution is nearly centered on the quiescent profile and has a similar shape. The total integrated ELM particle flux should not be correlated with the number of particles lost from the main plasma as the ejected particles must certainly recycle a number of times.

6. DIVERTOR MATERIAL STUDIES

The Divertor Material Evaluations Studies (DiMES) hydraulic mechanism allows insertion and retraction of graphite samples into the divertor floor of DIII–D. The samples are implanted with a Si depth marker in order to measure the net erosion or redeposition of the graphite [63-64]. Thin (100 nm) metal films of beryllium, vanadium, molybdenum and tungsten are also deposited on the samples to study the erosion, transport and redeposition properties of these trace metals in the all carbon plasma-facing environment of DIII–D. Figure 5 shows that the net loss of the carbon increases with increasing incident heat flux. These results were obtained during ELM-free and ELMing plasmas using both depth-marking [65] and colorimetry [66]. The REDEP code [67,68] has been used to simulate the measured net erosion at

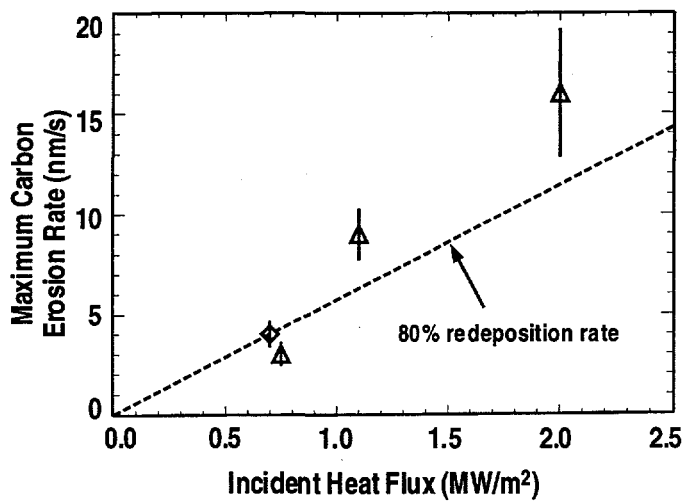

Fig. 5. Measured net carbon loss rate at DIII–D outer strike point vs. incident heat flux measured by infrared thermography. Δ — ELMing H–mode, ◊ — ELM-free H–mode. Dashed line is extrapolated net erosion rate from REDEP calculated 80% redeposition rate of ELM-free H–mode case.

0.7 MW/m^2. The code results show a gross erosion rate 5 times higher than the net, indicating a redeposition rate of 80%. At higher heat flux the net erosion is larger than the extrapolated value using this redeposition rate, indicating that the redeposition rate could be decreasing. This is despite the expected increase in local redeposition due to the increased divertor plasma density at the higher heat flux. The reason for this decreased redeposition may be linked to the ELMing behavior and studies are currently underway to explain this effect. One of the current ITER calculations for carbon divertor plate lifetimes [69] (90% redeposition, no angular dependence, loss rate ≈ 2 nm/s at 2.5 MW/m^2) are more optimistic than these measured rates, however a better understanding on the roles of ELMs, density and geometry (e.g. oblique incidence) are needed for a true comparison.

The toroidal redeposited pattern of the metals has shown that the e-folding length of the metals decreases with increasing atomic number, and also ionization rate, as expected. A WBC code [70] Monte-Carlo simulation obtains good agreement with the experimental data indicating that an adequate understanding of the sputtering geometry, the ionization processes and the ion trajectories exists. The loss rates of the metal films are difficult to interpret due to the highly perturbing effect of the 1%–2% carbon background plasma depositing and eroding onto the metals. However, the measured trend of decreasing sputtering yield for increasing atomic number is in agreement with predicted sputtering yields for these materials [65].

7. SUMMARY

In summary, we have measured the plasma parameters over the entire cross section of the divertor plasmas which for the first time allow local transport studies in the divertor plasmas. It is found that detached plasmas display a complicated pattern of momentum and radiative heat loss along the field lines. Spectroscopic evidence, consistent with the measured plasma parameters and UEDGE modeling show evidence of copious volume recombination in detached plasmas. Furthermore, our analysis

shows strong evidence of heat convection towards the divertor plate that in some cases greatly exceeds parallel electron heat conduction.

In several experiments we have utilized divertor pumping as an active tool for enhancing the plasma performance. A combination of gas puffing and divertor pumping was used to enrich impurity content of divertor plasmas and to obtain an extended divertor radiation zone. In the first experiment, based on direct measurements of neon and argon concentrations in the core plasma and pumping plenum, we have concluded SOL flows can increase divertor plenum impurity enrichment. In the second experiment we have observed nearly uniform radiation in the poloidal direction from the X–point to the target plate. This result is not consistent with purely classical parallel heat conduction and coronal equilibrium radiation. Thus we have concluded that convection and deviations from equilibrium must play a significant role in these plasmas. We also suspect the ELM heat pulse may transiently shift the radiative zone downstream. Divertor pumping in conjunction with pellet injection was used to overcome the divertor power balance limit and thus increase the core plasma density well beyond the Greenwald limit. We have achieved H–mode densities 1.5 times the Greenwald limit and L–mode densities as high as 3 times the limit. Finally, we have demonstrated that divertor pumping during the plasma shot can effectively replace He glow discharge cleaning (HeGDC), normally used between plasma shots to obtain high confinement.

From both our transport studies and performance enhancement experiments we conclude that SOL flows contribute significantly to the dynamics of heat and particle transport. Furthermore we have demonstrated that by a combination of gas puffing and divertor pumping forced flows can be generated which can be used to modify transport to our advantage, while maintaining the desired core plasma density. Taken together, these results show that the behavior of a divertor plasma near detachments departs from the conventional picture of a conduction limited heat flow and constant impurity fraction. The emerging picture appears far more favorable for the success of a radiative divertor.

ACKNOWLEDGMENT

This work was supported by the U.S. Department of Energy under Contract Nos. DE-AC03-89ER51114, DE-AC05-96OR22464, W-7405-ENG-48, W-31-109-ENG-38, DE-AC04-94AL85000, and Grant No. DE-FG03-95ER54294.

REFERENCES

[1] FENSTERMACHER, M.E. et al., Comprehensive 2D measurements of radiative divertor plasmas in DIII–D, in Proc. of 12th Conf. Plasma Surface Interactions, St. Raphael, France 1996, to be published in the J. Nucl. Mater.

[2] PETRIE, T.W., et al., Investigation of rlectron parallel pressure balance in the scrape-off layer of deuterium-based radiative divertor discharges in DIII–D, *ibid.*

[3] ALLEN, S.L.et al., Measurements of T_e and n_e with divertor Thomson scattering in radiative divertor discharges on DIII–D, in Proc. of 12th Conf. Plasma Surface Interactions, St. Raphael, France 1996, to be published in the J. Nucl. Mater.

[4] WATKINS, J.G., et al, Reciprocating and fixed probe measurements of n_e and T_e in the DIII–D divertor, *ibid* .

[5] JACKSON, G.L., et al., Impurity control for enhanced divertor and edge radiation in DIII–D discharges, *ibid.*
[6] NILSON, D.G, et al., Divertor Thomson scattering on DIII–D, to be published in Fusion Engineering and Design.
[7] CARLSTROM, T.N., et al., Initial operation of the divertor Thomson scattering diagnostic on DIII–D, in Proc. of the 11th Int. Conf. on High Temperature Plasma Diagnostics, Monterey, California, 1996, to be published.
[8] LEONARD, A.W., et al., Rev. Sci. Instrum. **66** (1995) 1201.
[9] FENSTERMACHER, M.E., et al., A tangentially viewing visible TV system for the DIII–D divertor, to be published in Rev. Sci. Instrum,
[10] WOOD, R.D., et al., Measurement of divertor impurity concentrations on DIII–D, in Controlled Fusion and Plasma Physics (Proc. of the 23rd Euro. Conf., Kiev, 1996) (European Physical Society, Petit-Lancy, 1996) (in press).
[11] MOYER, R.A.., et al., The role of turbulent transport in DIII–D scrape-off layer and divertor plasmas, in Proc. of 12th Conf. Plasma Surface Interactions, St. Raphael, France 1996, to be published in the J. Nucl. Mater.
[12] LASNIER, C.J., et al., Characteristics of the scrape-off layer in DIII–D high-performance negative central magnetic shear discharges, *ibid.*
[13] ROGNLIEN, T., et al., A fully implicit, time dependent 2D fluid code for modeling tokamak edge plasmas, J. Nucl. Mater. **196-198** (1992) 347.
[14] PORTER, G.D., et al., Divertor characterization experiments and modeling in DIII–D, Controlled Fusion and Plasma Physics (Proc. of the 23rd Euro. Conf., Kiev, 1996) (European Physical Society, Petit-Lancy, 1996) (in press).; PORTER, G.D., et al., Simulation of experimentally achieved DIII–D detached plasmas using the UEDGE code, Phys. Plasmas **3** (1996) 1967.
[15] FENSTERMACHER, M.E., UEDGE and DEGAS modeling of the DIII–D scrape-off layer plasma, J. Nucl. Mater. **220–222** (1995) 330.
[16] EVANS, T.E., et al., Monte-Carlo impurity transport simulations in the edge of the DIII–D tokamak using the MCI code, in Proc. 10th Int. Conf. on Stellarators, Madrid, Spain, to be published.
[17] Ohyabu., et al., Density oscilations in the tokamak plasma boundary with an expanded divertor channel, General Atomics Report GA-A16484 (1982).
[18] WEST, W.P., et al., Divertor plasma studies on DIII–D: experiment and modeling," Controlled Fusion and Plasma Physics (Proc. of the 23rd Euro. Conf., Kiev, 1996) (European Physical Society, Petit-Lancy, 1996) (in press).
[19] PETRIE, T.W., et al., Controlled Fusion and Plasma Physics (Proc. of the 18th Euro. Conf., Berlin, 1990 (European Physical Society, Petit-Lancy, Switzerland, 1991) Vol. 3, p. 237.
[20] HILL, D.N., et al., Divertor plasma studies on DIII–D, in Proc. 13th Int. Conf. on Plasma Physics and Contr. Fusion Research, (International Atomic Energy Agency, Vienna, 1991), Vol. 3, p. 487
[21] PETRIE, T.W., et al., J. Nucl, Mater. **196–198** (1992) 848.
[22] JANESCHITZ, G., et al., J. Nucl. Mater. **220–222** (1995) 73.
[23] WATKINS, M., and REBUT, P., Controlled Fusion and Plasma Physics (Proc. of the 19th Euro. Conf., Innsbruck, Austria (European Physical Society, Petit-Lancy, Switzerland, 1991) Vol. 16C, Part II, p. 731.
[24] JANESCHITZ, G., et al., J. Nucl, Mater. **220–222** (1995) 73.
[25] MATTHEWS, G.F., J. Nucl. Mater. **220–222** (1995) 104.
[26] PETRIE, T.W., et al., Radiative divertor experiments in DIII–D with D_2 injection, J. Nucl. Mater. **196-198** (1992) 848.

[27] KALLENBACH, A., et al., Nucl. Fusion **35** (1995) 1231.
[28] MAHDAVI, M.A., et al., J. Nucl. Mater. **220–222** (1995) 13.
[29] MAINGI, R., et al., J. Nucl. Mater. **220–222** (1995) 320.
[30] GHENDRIH, P., et al., Phys. Plasmas **1** (1994) 1929.
[31] SCHAFFER, M.J., et al., Pfirsch Schlueter, currents in the JET divertor, to be published in Nucl. Fusion.
[32] STAMBAUGH, R.D., et al., in Proc. 15th Int. Conf. on Plasma Physics and Contr. Fusion Research , Seville, Spain (International Atomic Energy Agency, Vienna, 1995), Vol. 1, p. 83.
[33] ISLER, R., et al., Spectroscopic characterization of the DIII–D divertor, to be published in Phys. Plasmas.
[34] WEST, W.P., et al., Modeling of impurity spectroscopy in the divertor and SOL of DIII–D using the 1-D multifluid model NEWT1D, in Proc. of the Int. Conf. on Plasma Physics, Nogoya, Japan, 1996, to be published.
[35] MAHDAVI, M.A., et al., Phys. Rev. Lett. **47** (1982) 1062.
[36] NEUHAUSER, J., et al., Nucl. Fusion **24** (1984) 39.
[37] MAHDAVI, M.A., et al., J. Nucl. Mater. **111–112** (1982) 355.
[38] BOSCH, H.-S., et al., Phys. Rev. Lett. **76** (1996) 2499.
[39] SCHAFFER, M.J., et al., Nucl. Fusion **35** (1995) 1000.
[40] SCHAFFER, M.J., et al., Direct measurement of divertor neon enrichment in DIII–D, in Proc. 12th Conf. Plasma Surface Interactions, St. Raphael, France, 1996, to be published in J. Nucl. Mater.
[41] WADE, M.R., et al., Phys. Plasmas **2** (1995) 2357.
[42] WADE, M.R., et al., Phys. Rev. Lett. **74** (1995) 2702.
[43] CAROLAN, P.G., and PIOTROWICZ, V.A., Plasma Phys. **25** (1983) 10.
[44] ALLEN, S.L., et al., J. Nucl. Mater. **196–198** (1992) 804.
[45] POST, D., et al., J. Nucl. Mater. **220–222** (1995) 1014.
[46] MAHDAVI, M.A., et al., Stability of a radiative mantle in ITER, in Proc. of 12th Conf. on Plasma Surface Interactions, St. Raphael, France, 1996, to be published.
[47] LEONARD, A.W., et al., Distributed divertor radiation through convection in DIII–D, submitted to Phys. Rev. Lett.
[48] MAHDAVI, M.A., et al., Controlled Fusion and Plasma Physics (Proc. 20th Euro. Conf., Lisboa, Portugal) (European Physical Society, Petit-Lancy, Switzerland, 1993) Vol. 17C, p. 647.
[49] MAINGI, R., et al., Comparison of wall/divertor deuterium retention and plasma fueling requirements on the DIII–D, TdeV, and ASDEX-Upgrade tokamaks, in Proc. of 12th Conf. on Plasma Surface Interactions, St. Raphael, France, 1996, to be published.
[50] MAINGI, R., et al., Nucl. Fusion **36** (1996) 245.
[51] GRENNWALD, M., et al., Nucl. Fusion **28** (1988) 12.
[52] BORRASS, K., Nucl. Fusion **31** (1991) 6.
[53] PETRIE, T.W., et al., Nucl. Fusion **33** (1993) 929.
[54] GIBSON, A., Nucl. Fusion **16** (1976) 546.
[55] PERKINS, F., this conference.
[56] BAKER, D.R., et al., Nucl. Fusion **22** 807 (1982).
[57] LEONARD, A.W., et al., Divertor heat and particle flux due to ELMs in DIII–D and ASDEX-Upgrade,in Proc. of 12th Conf. Plasma Surface Interactions, St. Raphael, France 1996, to be published in the J. Nucl. Mater.
[58] GOHIL, P., et al., Phys. Rev. Lett. **61** (1988) 1603.
[59] ZOHM, H., et al., Plasma Phys. and Contr. Fusion Research **36** (1994) 1307 .

[60] ZOHM. H., et al., Nucl. Fusion **35** (1995) 543.
[61] DIETZ, K.J., et al., in Proc. 15th Int. Conf. on Plasma Phys. and Contr. Nucl. Fusion Research 1994, Seville, Spain (International Atomic Energy Agency, Vienna, 1995) Vol. 2, p. 491.
[62] EVANS, T.E., et al., J. Nucl. Mater. **220–222** (1995) 235.
[63] BASTASZ, R., et al., J. Nucl. Mater. **220–222** (1995) 310.
[64] WAMPLER, W.R., et al., Erosion and deposition of metals and carbon in the DIII–D divertor, in Proc. 7th Int. Conf. on Fusion Reactor Materiaals, Obninsk, Russia, 1995, to be published in J. Nucl. Mater.
[65] WHYTE, D.G., et al., DiMES divertor erosion experiments on DIII–D, in Proc. 12th Conf. Plasma Surface Interactions, St. Raphael, France, 1996, to be published in J. Nucl. Mater.
[66] WESCHENFELDER, F., et al., In-situ measurement of erosion/deposition in the DIII–D divertor by colorimetry, Controlled Fusion and Plasma Physics (Proc. 22nd Euro. Conf., Bournemouth, 1995) (European Physical Society, Petit-Lancy, Switzerland, 1995) Vol. II, p. 281.
[67] HUA, T.Q., and BROOKS, J.N., J. Nucl. Mater. **220–222** (1995) 342.
[68] BROOKS, J.N., Nucl. Tech./Fusion 4 (1983) 33.
[69] JANESCHITZ, G., et al., J. Nucl. Mater. **220–222** (1995) 73.
[70] BROOKS, J.N., Phys. Fluids **8** (1990) 1858.